Eur. Phys. J. D (2015) 69: 48
DOI: 10.1140/epjd/e2015-50650-6

THE EUROPEAN PHYSICAL JOURNAL D

Regular Article

Multiplasmon excitations in electron spectra of small systems irradiated by swift charged projectiles

Phuong Mai Dinh[1,2,a], Paul-Gerhard Reinhard[3], Eric Suraud[1,2], and Philipp Wopperer[1,2]

[1] Université de Toulouse, UPS, Laboratoire de Physique Théorique (IRSAMC), 31062 Toulouse, France
[2] CNRS, LPT (IRSAMC), 31062 Toulouse, France
[3] Institut für Theoretische Physik, Universität Erlangen, 91058 Erlangen, Germany

Received 1st September 2014 / Received in final form 16 December 2014
Published online 17 February 2015 –

Abstract. We investigate the kinetic-energy spectrum of electrons emitted from an excited many-electron system, often called photo-electron spectrum (PES). We are particularly interested on the impact of resonant modes of the system on PES. To this end, we consider three systems with strong resonances, a Mg atom, the small alkaline cluster K_9^+, and the small carbon chain C_3. To avoid dominant frequencies in the excitation process, we consider a collision with a fast ion which is realized by an instantaneous boost of the valence electrons, a process which excites all frequencies with equal weight. The electron dynamics is investigated from a theoretical perspective using time-dependent density-functional theory augmented by an average-density self-interaction correction. We observe patterns which are similar to PES usually obtained after irradiation by a laser pulse, in particular the appearance of clear peaks. We show that these patterns are driven by strong resonance modes of the system. Resonances are thus found to be another source of peaks in the PES, besides photons (when present) with definite frequencies.

1 Introduction

Photo-electron spectra (PES) are a widely used and powerful observable to analyze electronic systems [1,2]. The conceptually simplest setup is to use a photon pulse with a well defined frequency which is sufficiently high in energy to ionize a great amount of single electron states by a one-photon excitation. This provides a direct map of the single-particle (s.p.) energies, for example from cluster physics, see [3,4]. More involved is the interpretation in the regime of multi-photon ionization (MPI) where PES can contain multiple copies of the s.p. spectra according to different photon numbers, often overlaid by thermal emission [5]. As a further contributor to PES, one often finds traces of the pronounced surface plasmon modes. Plasmon satellites are observed experimentally in X-ray PES of bulk metals [6], metal clusters [7,8], nested fullerenes [9], and C_{60} [10]. A competition between photon and plasmon peaks in metal clusters was also worked out theoretically for MPI with typical laser frequencies in reference [11]. It is, however, not always easy in the PES to disentangle peaks due to plasmon modes, or other strong resonances, from photon signals. In order to distill the effect of resonant modes, we choose an excitation which in itself has no frequency bias. This is achieved by very fast electromagnetic pulses as they are delivered by Coulomb collisions with fast ions. We model them in practice by an instantaneous boost of all valence electrons which excites all frequencies with equal weight, such that pronounced frequencies in the PES can only stem from the target molecule. This allows one to see the impact of strong modes on the PES more unambiguously than in the case of a laser excitation.

Collision experiments are still comparatively rare. Nonetheless, there exist already a few promising measurements which resolve properties of the emitted electrons, e.g. for collision of protons on uracil delivering total cross-sections and PAD [12,13] as well as PES [14]. These experiments are still lacking proper theoretical analysis, but they will certainly bring invaluable information on dynamical mechanisms by such a detailed analysis of the properties of emitted electrons. At present, even a theoretical proof of principle would bring a helpful piece of information. Thus it is the aim of this paper to investigate the impact of resonant modes on PES from a theoretical side. The fast collisional process is modeled in a simple manner by an instantaneous dipole boost of the electron cloud. The possible availability of more collision experiments is a strong motivation for the present paper. As test cases, we consider three rather different systems, that is, the Mg atom, the metal cluster K_9^+, and the C_3 chain. They however possess the common feature of being sufficiently metallic in the sense that their optical spectra are dominated by collective modes, as will be discussed at length for each case.

[a] e-mail: dinh@irsamc.ups-tlse.fr

The paper is outlined as follows: the theoretical and numerical background is sketched in Section 2. Results for the Mg atom are discussed in Section 3, for the K_9^+ cluster in Section 4, and for the C_3 chain in Section 5. We finally draw some conclusion in the last section.

2 Theory and numerical scheme

2.1 Dynamical simulation

We describe the electronic dynamics by means of real-time time-dependent density functional theory (TDDFT) in a standard manner [15,16]. We solve the (time-dependent) Kohn-Sham equations for the valence electrons on a grid in coordinate space, using time-splitting for time propagation [17] and accelerated gradient iterations for the stationary solution [18]. The Poisson equation is solved by a fast Fourier technique combined with separate treatment of the long-range terms [19]. We use the exchange-correlation energy functional from Perdew and Wang [20]. A self-interaction correction (SIC) has to be applied to obtain correct single particle (s.p.) energies which are crucial for an appropriate dynamical description of electron emission. We include it by the technically inexpensive Average-Density SIC (ADSIC) [21]. The coupling to the ions is mediated by soft local pseudopotentials in the case of Mg and K [22], and Goedecker-like ones in the case of C [23]. We use absorbing boundary conditions [15,16,24] which gently absorb all outgoing electron flow reaching the bounds of the grid and thus prevent artifacts from reflection back into the reaction zone.

Calculations for the Mg atom were done on a cylindrical grid extending $110a_0$ along the z(=symmetry) axis and $55a_0$ in r direction, with a mesh size of $0.5a_0$. The K_9^+ cluster is also treated in cylindrical symmetry in a box of mesh size of $0.9a_0$, and of length $200a_0$ in z and $100a_0$ in r. In this case, the cylindrical symmetry for the Kohn-Sham potential is an approximation, the cylindrically averaged pseudopotential scheme [25,26], which has proven to be an efficient and reliable approximation for metal clusters close to axial symmetry. The C_3 chain is computed on a three-dimensional grid with box lengths of $70a_0$ in each spatial direction, and a mesh size of $0.7a_0$.

2.2 Ionic collisions and instantaneous boost

The excitation mechanism used throughout this paper is an instantaneous dipole boost which is applied to all occupied single electron states j. For example, a boost by p_z in z-direction reads $\varphi_j(\mathbf{r}, t=0) = \exp(\mathrm{i}p_z z)\varphi_{j,\mathrm{gs}}(\mathbf{r})$ where $\varphi_{j,\mathrm{gs}}$ are the ground-state wave functions. This approximately models the effect of the Coulomb field of a fast charged projectile passing by. A sufficiently fast ion moves near the molecule practically on a straight line with constant velocity v. Let us assume that the ion moves orthogonal to the z axis in a frame whose origin lies at the molecule's center. The point of closest approach then lies on the z axis at a distance b, identical with the impact parameter. The Coulomb field of the ion exerts a force on the molecule electrons. Integrating the force over the collision process, we find that the net force has only a component in z direction [27]. For a sufficiently remote impact parameter b, the force field at the molecule site is practically homogeneous and boosts the electron momentum by

$$p_z = 4Ze^2/(bv) \tag{1}$$

where Z is the charge of the projectile and e the electron charge. Let us consider typical orders of magnitude for the maximally amenable boost momentum p_z. One condition is that the ionic velocity has to be large such that the passage is much shorter than the electronic reaction time. The time for the passage is of order $\delta t = b/v$. This has to be shorter than the relevant reaction times $\omega_{\mathrm{el}}^{-1}$. Thus we require $v/b \gg \omega_{\mathrm{el}}$. For a rough estimate, we assume $\omega_{\mathrm{el}} = 1$ Ry and an impact parameter $b = 10a_0$ which should stay outside the cluster's electron cloud. The limiting value for v is then $v = b\omega_{\mathrm{el}} = 10\,\mathrm{Ry}a_0 = 200a_0/\mathrm{fs}$. For a colliding proton, this corresponds to $E_{\mathrm{kin,p}} = 0.7$ MeV. More interesting is the corresponding boost strength. Inserting the $b = 10a_0$ and $v = 10\,\mathrm{Ry}a_0$ into the above formula for p_z yields $\delta p_z = 0.08Z/a_0$. With $Z = 1$ (proton), this is in the range of boosts used later. The estimate is at the optimistic side. One will probably need somewhat larger b and v. This reduces the achievable p_z. However, there is still the option to consider ions with higher charge states Z. This allows one to tune the boost strength in a wider range. In the following, we will work out a range of boost strengths where resonant effects on PES are visible.

2.3 Extracting observables

Optical response, that is, the photo-absorption strength distribution, constitutes the basic information on the collective modes and the particle-hole excitations of a system. We will compute the dipole strength distribution tracking the dipole signal following a faint instantaneous boost and subsequent spectral analysis, i.e. Fourier transforming the time-evolution of the dipole moment into the frequency domain [28].

The observable in the focus of this paper is the kinetic-energy spectrum of electrons emitted after the boost. In analogy to laser experiments, we call that a photo-electron spectrum (PES). It is computed in the same simple fashion as done in the first studies of laser excitations [29]. Note that strong and/or long laser pulses require more elaborate techniques [30] which are fortunately ignorable for the instantaneous excitations considered here. We choose a couple of "measuring points" $\mathbf{r}_{\mathcal{M}}$ far away from the emitting system and just before the absorbing boundaries. Out there, the Kohn-Sham field can be considered negligible and a free-particle dynamics can be assumed. Moreover, the closeness of the absorbing bounds allows one to assume that only outgoing waves with momentum $\mathbf{k} = k\mathbf{r}_{\mathcal{M}}/r_{\mathcal{M}}$ and $k > 0$ pass the point $\mathbf{r}_{\mathcal{M}}$. We now record a protocol of each s.p. wave functions $\varphi_j(\mathbf{r}_{\mathcal{M}}, t)$ during simulation. As we encounter practically outgoing free waves at

the $\mathbf{r}_{\mathcal{M}}$, the kinetic-energy content of the wave function is equivalently contained in the frequency spectrum of the wave functions. The PES yield $\mathcal{Y}_{\Omega_{\mathbf{r}_{\mathcal{M}}}}(E_{\rm kin})$ can thus be obtained from Fourier transformation from time to frequency ω of φ_j as:

$$\mathcal{Y}_{\Omega_{\mathbf{r}_{\mathcal{M}}}}(E_{\rm kin}) \propto \sum_{j=1}^{N} \left|\widetilde{\varphi}_j(\mathbf{r}_{\mathcal{M}}, E_{\rm kin})\right|^2, \qquad (2)$$

where $\Omega_{\mathbf{r}_{\mathcal{M}}}$ is the solid angle related to the direction of $\mathbf{r}_{\mathcal{M}}$, and $\widetilde{\varphi}_j(\mathbf{r}_{\mathcal{M}}, E_{\rm kin})$ is the time-frequency Fourier transform of the wave function of state j, $\varphi_j(\mathbf{r}_{\mathcal{M}}, t)$, with $E_{\rm kin} = k^2/2m_e = \omega$ [29,30]. Each term in the sum of equation (2) represents the PES for emission from a single state j. Such a state-specific PES can be used for analyzing the results. Moreover, taking a sufficiently fine mesh of measuring points $\mathbf{r}_{\mathcal{M}}$ allows one to evaluate the angular-resolved PES. In the present paper, we will mostly consider angular-averaged PES, i.e., the PES according to equation (2) averaged over all $\mathbf{r}_{\mathcal{M}}$ with appropriate angular weights, and discuss an energy- and angle-resolved PES only in the case of C_3. Although the boost is a fast excitation, electron emission and accumulation of PES take a while because slow electrons reach the measuring points late. Computations were carried forth long enough to cover a large fraction of emitted electrons, from 64 fs for the C chain up to 300 fs for the K cluster.

3 A simple example: the Mg atom

As a starter, we choose the simple and oversee-able example of a single Mg atom to investigate the effect of dominant excitation modes on the PES after instantaneous excitation. The Mg atom is ideal for our purposes because it has a single valence state ($E_{\rm IP} = 7.6$ eV experimentally [31], 8 eV in our calculations) and it has a strong $2s \longrightarrow 2p$ dipole transition which dominates the spectrum by far. This can be seen from the photoabsorption spectrum in the inset of Figure 1, with the peak labeled ω_1. One can, however, notice further smaller excitation states following at higher energies. Among them, the second transition, marked by ω_2, has still a sizable strength, and we will see in the following that it does play a role in the PES. Note also that most of the optical response of the Mg atom lies below the ionization potential (IP).

In spite of the fact that the instantaneous boost excitation covers a continuous spectrum of frequencies, the PES clearly shows distinctive peaks above background, as can be seen from Figure 1. The kinetic energies $E_{\rm kin}$ at which the most prominent peaks of the PES occur can be associated with the strongly excited states according to the rule:

$$E_{\rm kin} = \varepsilon_j + \sum_{k=1}^{M} \nu_k \omega_k, \qquad (3)$$

where ε_j denotes the s.p. energy of orbital j, the integer k runs over the M various strong modes inferred from the optical response, and ν_k are integers. This looks similar to the rule $E_{\rm kin} = \varepsilon_j + \nu\omega_{\rm las}$ which applies if the system is excited by a laser pulse with frequency $\omega_{\rm las}$. The difference is that the photon frequency $\omega_{\rm las}$ is imposed from outside the system while here in equation (3) the dominant frequencies are system properties. In the situation displayed in Figure 1, we have for the Mg atom $M = 2$ because there are 2 dominant peaks in the optical response (see inset), and the coefficients ν_1 and ν_2 can take values from 0 to 3 (for instance, the last peak indicated by a vertical line in the PES corresponds to $\nu_1 = 2$ and $\nu_2 = 1$). As expected, the peak height in the PES is related to the strength of each mode: the highest peaks are associated to a double and a triple plasmon excitation of ω_1, while the peaks raising from linear combinations of ω_1 and ω_2 show smaller relative heights, either in the case of a double plasmon excitation or a triple one.

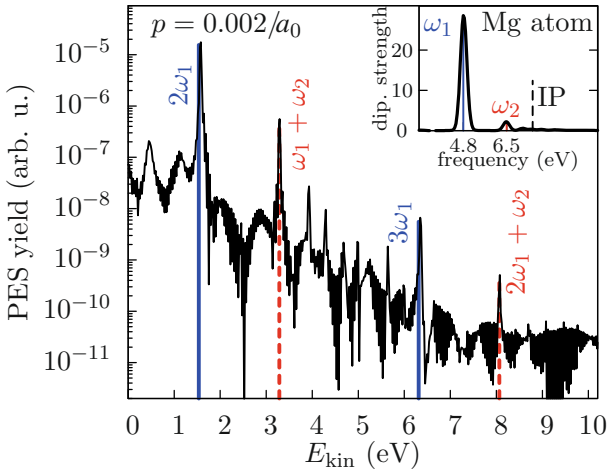

Fig. 1. Calculated photoelectron spectrum of the Mg atom after an excitation by an instantaneous boost of $0.002/a_0$. The vertical lines emphasize the kinetic energies as given by equation (3). Inset: dipole strength (in vertical linear scale and arbitrary units) with two dominant peaks located at $\omega_1 = 4.8$ eV and $\omega_2 = 6.5$ eV. The dashed line indicates the value of the ionization potential at 8 eV.

One can even further notice a couple of more peaks of smaller strength. They may be associated with the smaller peaks in the photo-absorption spectrum. But a detailed assignment according to equation (3) becomes soon untraceable because there are too many possible combinations of the various minor peaks. This example thus nicely demonstrates that strong excitations can be seen as peaks in the PES and that one needs rather dominant and distinct excitation modes for an unambiguous analysis.

4 The case of an alkaline cluster

Metal clusters are known for their prominent Mie surface plasmon [32]. However, this plasmon can be strongly fragmented due to interference with s.p. excitations in the case of heavier clusters [33]. Small clusters offer the best chances to encounter a clean excitation. Figure 2 shows

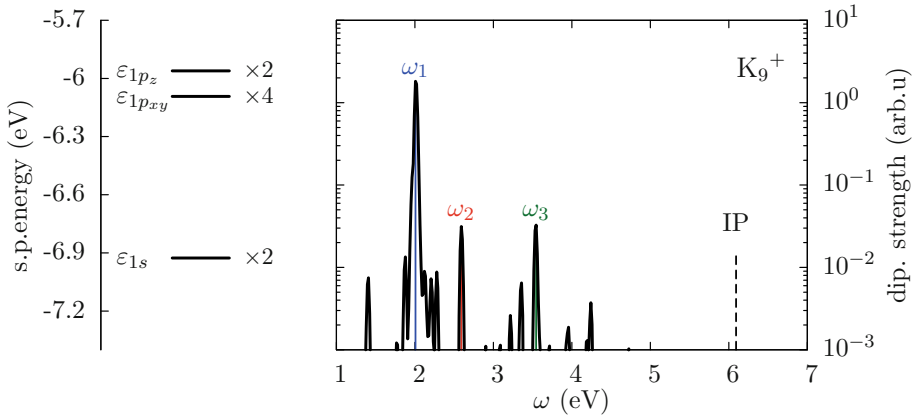

Fig. 2. Left: single particle (s.p.) energies of K_9^+ with degeneracies indicated at the right side of each level. Right: calculated optical response of K_9^+, with the three dominant frequencies labeled as $\omega_{1,2,3}$ and the ionization potential indicated by the vertical dashed line. The electronic density and the ionic structure of K_9^+ appear as an inset.

the dipole excitation spectrum (in logarithmic scale) of the K_9^+ cluster. The excitation spectrum is indeed dominated by the Mie surface plasmon associated here with the frequency denoted ω_1. But there is a couple of other dipole modes. The next two important ones are labeled by frequencies ω_2 and ω_3. We finally note that, as in the case of the Mg atom, the IP of K_9^+, at 6.1 eV, lies much above its optical response.

We now turn to the PES obtained after an instantaneous boost, see Figure 3. The upper panel shows the PES obtained with three different instantaneous boost momenta p as indicated. The total number of emitted electrons increases from 0.007 for the lowest boost $p = p_0 = 0.01/a_0$, up to 0.54 for $p = 40p_0$. Correspondingly, the peak structure gets more and more blurred with a steady downshift and a broadening of the peaks. As in previous studies [11], a total electronic emission of $\approx$1 seems to be the critical ionization where PES peaks become completely dissolved. This means that a clean signal can be obtained only in a very specific range of impact parameters: the boost should be large enough to raise the signal above background, but also small enough to avoid washing out the PES.

We thus discuss in more detail the smallest of the three boost excitations, since it delivers the cleanest signal: it yields a very small ionization which leaves the s.p. energies practically unchanged (the problem of the Coulomb shift from ionization and its impact on PES will be discussed in the next section). The two lower panels of Figure 3 show state-specific PES. The system has three groups of (degenerate) states, a deep lying twofold $1s$ state at $\varepsilon_{1s} = -6.9$ eV, and a slightly splitted group of $1p$ states with fourfold $\varepsilon_{1p_{xy}} = -6.1$ eV and twofold $\varepsilon_{1p_z} = -6.0$ eV. Emission from the $1p_z$ state is suppressed as compared to the two other states due to unfavorable coupling matrix elements. The figure thus shows only the two relevant contributions to the PES, the middle panel from $1p_{xy}$ and the lower panel from $1s$. The total PES is then the superposition of the two separate spectra.

Both PES show a variety of peaks which look at first glance rather puzzling. Of course, a cluster is more complex than a simple atom. Consequently, the PES is more involved. The various vertical lines in the plot indicate frequencies according to the rule (3) with $\varepsilon_j = \varepsilon_{1p_{xy}}$ in the middle panel and $\varepsilon_j = \varepsilon_{1s}$ in the lower one. We see that all larger peaks can uniquely be associated to a proper mix of excitation frequencies. The simplest way to explain peaks are those which contain just a multiple of the plasmon frequency ω_1 (see blue solid lines); they are indeed found to be prominent peaks in the total PES in the top panel of the figure, for a given ensemble of multi-mode excitation (4-plasmon excitation, 5-plasmon one, etc.). Apparently, the energy given by the boost to the cluster is first mainly stored in the collective plasmon and then, from time to time, transferred to single electrons. This is revealed, e.g. in the 4-plasmon excitation, by a peak at $\varepsilon_{1p_{xy}} + 3\omega_1 + \omega_2$ in the middle panel, and a peak at $\varepsilon_{1s} + 3\omega_1 + \omega_3$ in the bottom panel. Note also that for the 3-plasmon excitation, $3\omega_1$ is not sufficient to ionize the $1p_{xy}$ state. This is why we rather assign the peaks at low $E_{\rm kin}$ to excitations from $2\omega_1 + \omega_2$ or $2\omega_1 + \omega_3$.

This example on K_9^+ thus nicely demonstrates that the actual excitation spectrum has a direct impact on the PES. However, it also indicates that a metal cluster already produces a complex picture and it may not be straightforward to recover clear plasmon signals in collision experiments where we usually do not have the possibility to disentangle contributions from the separate states.

5 The C_3 chain

We now turn to the C_3 chain as a more complex system which is initially built on covalent binding, but which also exhibits partially metallic behaviour. Small carbon molecules can be produced in laboratory by thermal/laser vaporization of graphite or by electron impact induced fragmentation of hydrocarbons [34,35]. Among all physical properties, their structure has been under debate since long. Electron affinities measured by photoelectron spectroscopy as well as abundances show an even-odd alternation for size below 20 [36–38]. This supports the

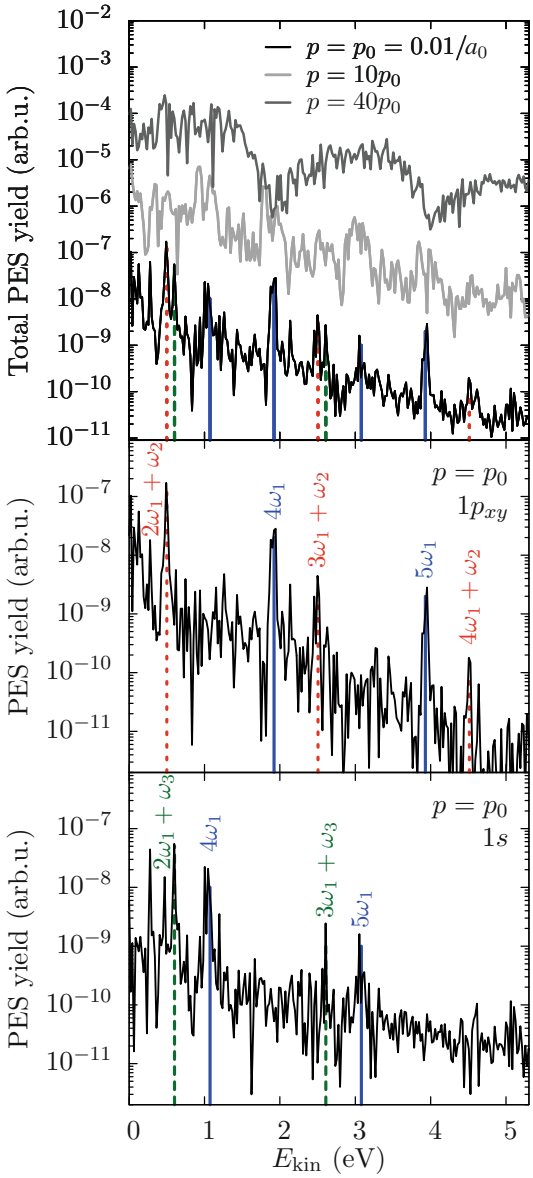

Fig. 3. Photoelectron spectra (PES) from instantaneous boost for a K_9^+ cluster. Upper: total PES for three boost strengths as indicated. The PES are rescaled to achieve a better visibility. Middle: PES from the $1p_{xy}$ state for boost momentum $p = p_0 = 0.01/a_0$. Lower: PES from the $1s$ state for boost momentum $p = p_0 = 0.01/a_0$.

assumption that linear chains are the predominant structure at these sizes since chains with odd numbers of atoms have closed-shell ground states, while chains with an even number of atoms have open-shell ones. For the purpose of this study, we focus on the smallest carbon chain, that is C_3. In the following, we first discuss the static properties of C_3 (energy spectrum and optical response) and then move to its PES produced by an instantaneous boost.

5.1 Static properties and optical response

The C_3 chain is a simple linear molecule. The C-C bond length of $2.414a_0$ used in our calculations agrees with previous theoretical results (between 2.415 and $2.485a_0$) [39–43]. The s.p. spectrum of C_3 as well as the degeneracy and labeling of each state is displayed in the left panel of Figure 4. The C_3 has 12 valence electrons which group into 5 (degenerated) states with a large gap of about 7 eV between the two deepest levels and the three higher ones. Our calculated value of the IP for C_3, $E_{\rm IP} = -\varepsilon_5 = 10.8$ eV, is in fair agreement with other calculations (12.0 eV [44,45]) and experimental measurements (11.6 eV [46], 12.1 eV [47], and 13.0 eV [48]). Our calculated IP is a bit too low. This is because we refitted the parameters of the Goedecker-like pseudopotential to allow us to use a mesh size of $0.7a_0$. If we use the original value of the Goedecker pseudopotential [23], we obtain an IP of 11.3 eV [49], much closer to the experimental value. However, that would mean a mesh size twice smaller ($0.36a_0$), that is huge numerical boxes which represent a great hindrance for the dynamical calculations we present here. So, there is indeed a dependence of the IP on the pseudopotential parameters that we use. However, too low an IP does not significantly impact the principle effects investigated here.

We now turn to the photoabsorption strength of C_3 shown on the right part of Figure 4. In contrast to the Mg atom and the K_9^+ cluster which are more or less spherically symmetric systems, the carbon chain looks and behaves very different in the longitudinal direction (along the symmetry axis = z axis) and the transverse one. The response in the transverse direction is suppressed with respect to that in the longitudinal direction. This is not surprising because the restoring forces are stronger for transverse modes, thus forcing smaller amplitudes. We also observe a strong spectral fragmentation in both directions. The strongest longitudinal mode resides at $\omega_1 = 8.4$ eV, closely followed (in position and strength) by another strong longitudinal mode at $\omega_2 = 8.8$ eV. These two modes together exhaust the dominant fraction of the longitudinal dipole strength. We expect that they should produce visible effects in the PES. The resonance frequency is in very good agreement with previous theoretical calculations ($\omega_1 = 8.1$ eV [50,51]). However, all theoretical results lie much higher than the measured plasmons: 7.3–7.8 eV [52] and 6.6 eV [53]. Again, we argue that this possible mismatch is no hindrance for the present and qualitative exploration.

It is finally worth mentioning that, even if ω_1 and ω_2 are below IP, there is a basic difference of C_3 compared with the Mg atom and the K_9^+ cluster: a still significant part of the dipole strength lies above the IP. These excitations reside in the electron continuum and emit directly, thus overlaying the signal from the (discrete) resonances. This indicates that a PES from an instantaneous boost might be more involved than in the two previous examples. This will be confirmed in the next section.

5.2 Multi-mode excitation peaks in PES

We now turn to the PES and PAD of C_3. To avoid interference with transverse modes, we apply the instantaneous

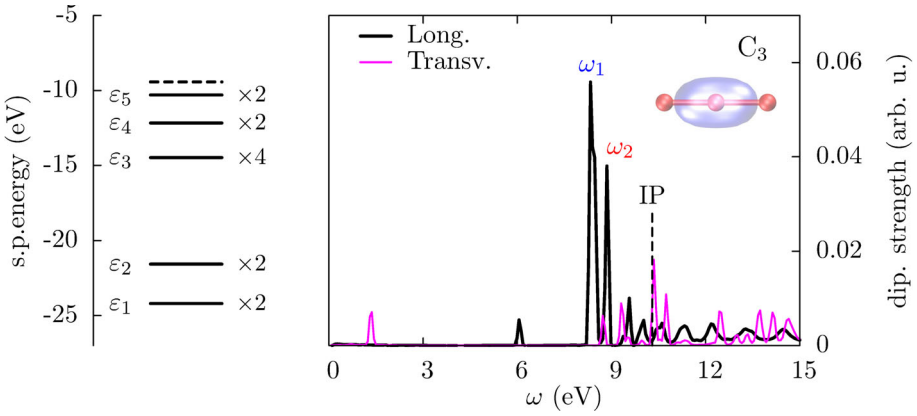

Fig. 4. Basic properties of the C_3 chain. Left: calculated single particle spectrum with degeneracies indicated at the right side of the levels, the numbering of states at the left. The dashed line represents the LUMO. Right: calculated optical response with the two strongest longitudinal modes associated with frequency labels $\omega_{1,2}$ and the position of the ionization potential (IP) indicated by a vertical dashed line. The ionic structure of C_3 with the electronic density appears as an inset.

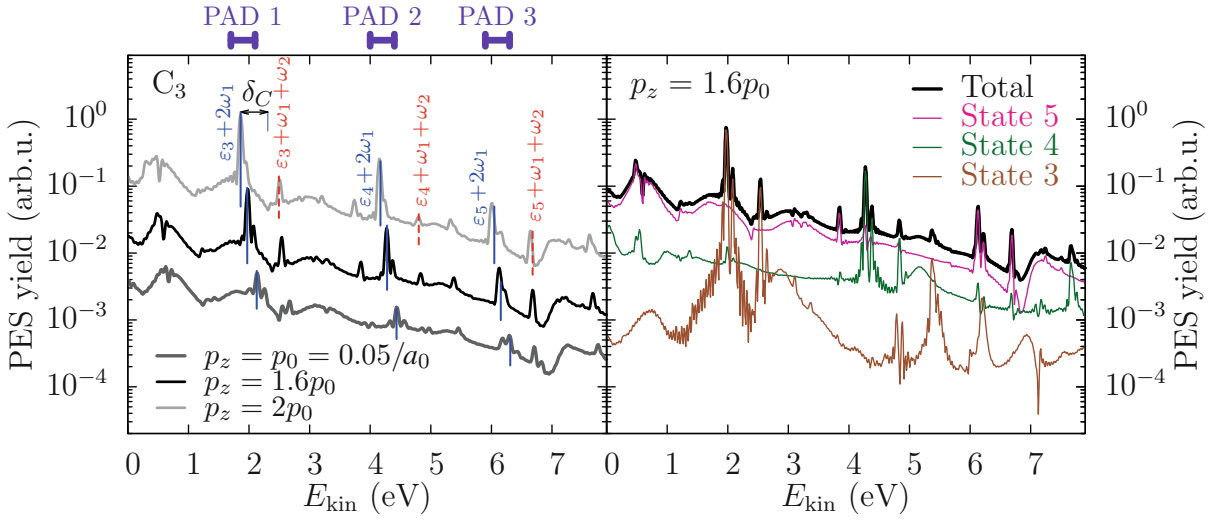

Fig. 5. Left: photoelectron spectra for C_3 excited by an initial instantaneous boost along longitudinal (z) direction with different boost strengths as indicated. Results are rescaled for better visualization. The vertical lines indicate expected $E_{\rm kin}$ according to equation (4) for $2\omega_1$-excitations (solid) and for $\omega_1+\omega_2$-excitations (dashes) of s.p. states labeled in Figure 4. Here, δ_C indicates a Coulomb shift of the peaks (see text for details). The horizontal bars marked by PAD i with $i = 1, 2, 3$ at the top indicate the energy regions over which the corresponding PAD are plotted in Figure 6. Right: state-resolved PES for boost $p = p_z = 1.6p_0$.

boost in the longitudinal (or z) direction only. The obtained PES are shown in the left panel of Figure 6 for three different boost momenta p_z, $p_0 = 0.05/a_0$, $1.6p_0$, and $2p_0$. We clearly see strong peaks sticking out of a noisy background. The vertical lines indicate the peak positions predicted by the rule (3), dashed lines for twice the ω_1 mode and dotted lines for a combination of ω_1 and ω_2. The assignments are corroborated by checking with the PES from specific states 3, 4, and 5, shown in the right panel of Figure 5. One can clearly identify which state produces which peak. The peaks in the total PES (left panel) show a trend with boost strength: they grow in height and are down-shifted to lower $E_{\rm kin}$ with increasing boost. The down-shift, also called "Coulomb shift", had already been observed before in connection with laser induced PES [29]. It is due to ionization. Note first that electron emission increases with boost strength: we find a total ionization $N_{\rm esc} = 0.018$, 0.05, and 0.082 for $p_0 = 0.05/a_0$, $1.6p_0$, and $2p_0$ respectively. This ionization deepens the Coulomb potential as $-N_{\rm esc}e/r$ in the course of the electron emission which, in turn, leads to the Coulomb shift of s.p. energies. Therefore, equation (3) must be modified to

$$E_{\rm kin} = \varepsilon_j + \sum_{k=1}^{M} \nu_k \omega_k - \delta_C, \tag{4}$$

where $\delta_C = N_{\rm esc}e/R_{\rm syst}$ stands for the Coulomb shift and $R_{\rm syst}$ is the relevant system radius. As is visible in Figure 5, a given peak is gradually redshifted, that is, δ_C increases with p_z. We have emphasized by an horizontal arrow the maximum value of δ_C (here, 0.44 eV) obtained for the strongest boost.

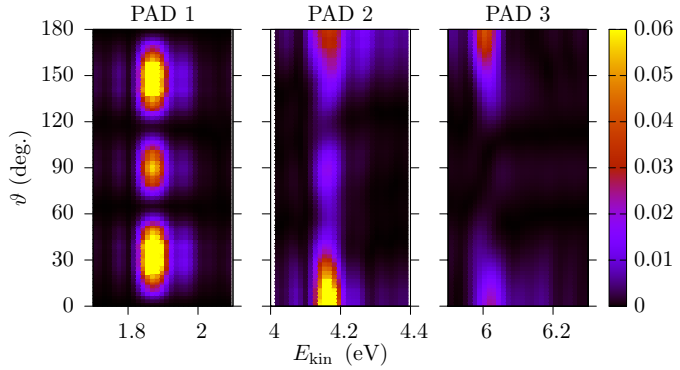

Fig. 6. Combined PES/PAD of C_3 for boost strength $p_z = 0.05/a_0$ in the three energy ranges as indicated in Figure 5.

Besides the Coulomb shift, the peaks grow with increasing boost. This indicates that they stem from non-linear effects, actually quadratic in the excitation. The background remains rather inert, except for the global upshift. This suggests that most of the background stems from direct emission by continuum modes. The many bumpy structures in the background reflect the fact that the dipole spectrum above IP is still rather structured, see right panel in Figure 4. These bumps are rather broad which confirms that they correspond to continuum states with large escape width. In contrast, the peaks from $2\omega_1$ processes are very narrow because truly bound modes are involved. Of course, for stronger excitations, there might also be other non-linear combinations of modes and some cross-talk to transverse modes. However, the spectral density of such events is large and the strength is weak. These secondary effects are probably dissolved in the background.

Finally, Figure 6 displays the combined PES/PAD zoomed onto the regions of the three prominent peaks as indicated in Figure 5. The 0 and 180° angles correspond to the longitudinal direction. Although the excitation is done along this axis, electrons are not emitted exclusively in this direction: the deeper bound the state, the less aligned the emission. Indeed, whereas PAD 3 (emission from the HOMO) exhibits a maximum at $\theta = 0$ and $\theta = 180°$, PAD 2 (emission from HOMO−1) possesses in addition a secondary maximum in the transverse direction ($\theta = 90°$). And for PAD 1, the emission is not aligned at all with the chain axis. It rather peaks at $\theta = 30°$ and 150°, with a local maximum at 90°. This appearance of state-specific sidewards emission indicates that the processes considered here still stay in a regime of moderate excitations. Further increased excitation will push emission more to forward direction [54]. But this happens at the price of washing out the PES, see Figure 3.

6 Conclusions

In this paper, we have explored the impact of strong resonance modes of an electronic system on the distribution of kinetic energies of emitted electrons, called Photo-Electron Spectrum (PES) in analogy to laser induced experiments. Test cases are the Mg atom, K_9^+ as a metal cluster, and the C_3 chain as a covalent molecule still exhibiting a partially metallic behavior. To eliminate any frequency bias from outside, we employ a short-time excitation process through collision with a fast charged projectile. The Coulomb field delivered by the bypassing ion is well described by an instantaneous dipole boost of the electronic wave functions. The resonant modes of the molecules have been determined by spectral analysis of the optical response in an independent calculation.

The resulting PES show sequences of pronounced peaks much similar to the case of laser excitation. But here the peaks have to be assigned as multi-plasmon (multi-resonance) excitations of the single particle states. Such an assignment is simple and obvious for the strongest resonance. It may be carried forth to secondary resonances if they are strong enough. Peaks with small strength and/or high spectral density disappear in the background signal. Henceforth, the conditions for the observation of these peaks are extremely demanding. One needs, first of all, a spectrum with one or two clearly dominating peaks which sets strong limits on possible systems. Even then, there is only a narrow window of excitation strength for the observation. For too weak an excitation (too large and impact parameter and/or too small a charge), the modes are not excited strongly enough to lift the peaks above background. For too strong an excitation (too small an impact parameter and/or too high a charge), the PES is smeared out as a consequence of the gradual downshift of the single particle spectrum. This also means that experimentally the excitation of multiple modes should be visible in a PES only for well selected sets of b, Z, and v.

This work was supported by the Institut Universitaire de France, and was granted access to the HPC resources of IDRIS under the allocation 2014–095115 made by GENCI (Grand Equipement National de Calcul Intensif), of CalMiP (Calcul en Midi-Pyrénées) under the allocation P1238, and of RRZE (Regionales Rechenzentrum Erlangen).

References

1. J. Berkowitz, *Photoabsorption, Photoionization and Photoelectron Spectroscopy* (Academic, New York, 1979)
2. P. Ghosh, *Introduction to photoelectron spectroscopy* (John Wiley and Sons, New York, 1983)
3. D.G. Leopold, J. Ho, W.C. Lineberger, J. Chem. Phys. **86**, 1715 (1987)
4. O. Kostko, N. Morgner, M.A. Hoffmann, B. von Issendorff, Eur. Phys. J. D **34**, 133 (2005)
5. E.E.B. Campbell, K. Hansen, K. Hoffmann, G. Korn, M. Tchaplyguine, M. Wittmann, I.V. Hertel, Phys. Rev. Lett. **84**, 2128 (2000)
6. A.P. Grosvenor, M.C. Biesinger, R.S. Smart, N.S. McIntyre, Surf. Sci. **600**, 1771 (2006)
7. T. Andersson et al., J. Chem. Phys. **134**, 094511 (2011)
8. T. Andersson, C. Zhang, M. Tchaplyguine, S. Svensson, N. Martensson, O. Bjorneholm, J. Chem. Phys. **136**, 204504 (2012)
9. M.A. McCune, R. De, M.E. Madjet, H.S. Chakraborty, S.T. Manson, J. Phys. B **44**, 241002 (2011)

10. E. Maurat, P.A. Hervieux, F. Lépine, J. Phys. B **42**, 165105 (2009)
11. A. Pohl, P.G. Reinhard, E. Suraud, J. Phys. B **34**, 4969 (2001)
12. A.N. Agnihotri et al., Phys. Rev. A **85**, 032711 (2012)
13. L. Tribedi, A. Agnihotri, M. Galassi, R. Rivarola, C. Champion, Eur. Phys. J. D **66**, 303 (2012)
14. A. Le Padellec, P. Moretto-Capelle, M. Richard-Viard, J.P. Champeaux, P. Cafarelli, J. Phys.: Conf. Ser. **101**, 012007 (2008)
15. F. Calvayrac, P.G. Reinhard, E. Suraud, C.A. Ullrich, Phys. Rep. **337**, 493 (2000)
16. P.G. Reinhard, E. Suraud, *Introduction to Cluster Dynamics* (Wiley, New York, 2003)
17. M.D. Feit, J.A. Fleck Jr., A. Steiger, J. Comput. Phys. **47**, 412 (1982)
18. V. Blum, G. Lauritsch, J.A. Maruhn, P.G. Reinhard, J. Comput. Phys. **100**, 364 (1992)
19. G. Lauritsch, P.G. Reinhard, Int. J. Mod. Phys. C **5**, 65 (1994)
20. J.P. Perdew, Y. Wang, Phys. Rev. B **45**, 13244 (1992)
21. C. Legrand, E. Suraud, P.G. Reinhard, J. Phys. B **35**, 1115 (2002)
22. S. Kümmel, M. Brack, P.G. Reinhard, Eur. Phys. J. D **9**, 149 (1999)
23. S. Goedecker, M. Teter, J. Hutter, Phys. Rev. B **54**, 1703 (1996)
24. P.G. Reinhard, P.D. Stevenson, D. Almehed, J.A. Maruhn, M.R. Strayer, Phys. Rev. E **73**, 036709 (2006)
25. B. Montag, P.G. Reinhard, Phys. Lett. A **193**, 380 (1994)
26. B. Montag, P.G. Reinhard, Z. Phys. D **33**, 265 (1995)
27. M. Bär, B. Jakob, P.G. Reinhard, C. Toepffer, Phys. Rev. A **73**, 022719 (2006)
28. F. Calvayrac, P.G. Reinhard, E. Suraud, Ann. Phys. **255**, 125 (1997)
29. A. Pohl, P.G. Reinhard, E. Suraud, Phys. Rev. Lett. **84**, 5090 (2000)
30. P.M. Dinh, P. Romaniello, P.G. Reinhard, E. Suraud, Phys. Rev. A **87**, 032514 (2013)
31. D.R. Lide, *Handbook of Chemistry and Physics* (Boca Raton, 2008)
32. U. Kreibig, M. Vollmer, in *Optical Properties of Metal Clusters*, Springer Series in Materials Science (Springer, 1993), Vol. 25
33. P.G. Reinhard, O. Genzken, M. Brack, Ann. Phys. (Leipzig) **508**, 576 (1996)
34. E.A. Rohlfing, D.M. Cox, A. Kaldor, J. Chem. Phys. **81**, 3322 (1984)
35. C. Lifshitz, Int. J. Mass Spectrom. **200**, 423 (2000)
36. W. Weltner Jr., R.J. Van Zee, Chem. Rev. **89**, 1713 (1989)
37. D.W. Arnold, S.E. Bradforth, T.N. Kitsopoulos, D.M. Neumark, J. Chem. Phys. **95**, 8753 (1991)
38. S. Yang, K.J. Taylor, M.J. Craycraft, J. Conceicao, C.L. Pettiette, O. Cheshnovsky, R.E. Smalley, Chem. Phys. Lett. **144**, 431 (1988)
39. D.P. Kosimov, A.A. Dzhurakhalov, F.M. Peeters, Phys. Rev. B **78**, 235433 (2008)
40. C. Zhang, X. Xu, H. Wu, Q. Zhang, Chem. Phys. Lett. **364**, 213 (2002)
41. M. Menon, K.R. Subbaswamy, M. Sawtarie, Phys. Rev. B **48**, 8398 (1993)
42. C.H. Xu, C.Z. Wang, C.T. Chan, K.M. Ho, J. Phys.: Condens. Matter **4**, 6047 (1992)
43. K. Raghavachari, J.S. Binkley, J. Chem. Phys. **87**, 2191 (1987)
44. S. Díaz-Tendero, F. Martín, M. Alcamí, J. Phys. Chem. A **106**, 10782 (2002)
45. X. Liang, Y.H. Luo, X.J. Feng, T.T. Cao, L.X. Zhao, Eur. Phys. J. D **46**, 93 (2008)
46. L. Belau, S.E. Wheeler, B.W. Ticknor, M. Ahmed, S.R. Leone, W.D. Allen, H.F. Schaefer III, M.A. Duncan, J. Am. Chem. Soc. **129**, 10229 (2007)
47. J. Benedikt, S. Agarwal, D. Eijkman, W. Vandamme, M. Creatore, M.C.M. van de Sanden, J. Vac. Sci. Technol. A **23**, 1400 (2005)
48. R. Ramanathan, J.A. Zimmerman, J.R. Eyler, J. Chem. Phys. **98**, 7838 (1993)
49. P. Klüpfel, P. Dinh, P.G. Reinhard, E. Suraud, Phys. Rev. A **88**, 052501 (2013)
50. K. Yabana, G.F. Bertsch, Z. Phys. D **42**, 219 (1997)
51. M. Kolbuszewski, J. Chem. Phys. **102**, 3679 (1995)
52. G. Monninger, M. Förderer, P. Gürtler, S. Kalhofer, S. Petersen, L. Nemes, P.G. Szalay, W. Krätschmer, J. Phys. Chem. A **106**, 5779 (2002)
53. K.W. Chang, W.R.M. Graham, J. Chem. Phys. **77**, 4300 (1982)
54. A. Pohl, P.G. Reinhard, E. Suraud, Phys. Rev. A **70**, 023202 (2004)